



doi:10.5281/zenodo.20282904

Integration of Geophysical Methods and Analytic Hierarchy Process in Assessment of Mineralization Zones of Gashu'a, Geidam, Dapchi and Biriri

Mohammed Mohammed¹, Muhammad Mustapha², Shehu Sherrif³.

**Department of Physics,
Umar Suleiman College of Education, Gashu'a, Yobe State., Nigeria
Email: msquare202004@gmail.com Cellphone: +2348033310748**

ABSTRACT

The study will depend on the use of multidisciplinary methods to characterize the aquifer in the area lying between the latitude 13⁰⁰'00''N to 12⁰⁰'00'' and longitude 12⁰⁰'00''N to 11⁰⁰'00''N. Aeromagnetic, Aeroradiometric and physicochemical methods will be deployed. The data will be reduced, analyzed and interpreted based on the geology of the area. The results of the interpretation will be cross-correlated and inferences regarding the characteristics of the mineralization will be deployed. Various software will be deployed to ensure optimal and reliable outcome are obtained. The findings of the study will reveal information about the in-depth features concealed regarding the Minerals and the environment within the study area.

Keywords:

INTRODUCTION

The major sources of raw materials for many industries around the world such as automobile, agriculture, pharmacy, electronic etc, are from mineral resources. Nigeria among other countries is blessed with vast mineral resources including gold, tin, iron, tantalite, limestone, kaolin and many more. The commercial value of Nigeria's mineral resources is estimated to reach hundreds of trillions of dollars (Jamaluddeen, Aku, Saleh, Bunawa, & Sharafa, 2019).

To uncover these subsurface mineral resources, various geophysical techniques such as magnetic, radiometric, electromagnetic, resistivity and gravity were deployed independently or combined. Akinlalu, Olayanju, Adiat, & Omosuyi (2021) used Aeromagnetic Data and AHP using Multi-criteria Decision Analysis to assessed mineral potential zones, the research shows a relatively very high degree of accuracy of the mineralisation potential map and thus confirming the reliability of the methodology adopted for this research.

Hussaini, et al. (2021) determine the depth to basement using spectral analysis of aeromagnetic data over azare segment of Chad basin, the result shows that depth to the deeper magnetic source ranges from 4503.9m to 1948.3m. However, it can be observed that NN, NE, and NW are having less deep magnetic sources ranging from 1948m to 2459.7m.

The deepest sources happened at the major towns of interest which are Bidawa, Matsango, Yakiri and Fatara areas, Katagum Bauchi state ranging from 2632.8m to 4503.9m the maximum depth of the sedimentary unit was estimated as 4.5km because the isolated value beyond this depth cannot be connected, and this depth occurs around Matsango and Bidawa. Chisambi, Haundi, & Ghambi (2023)

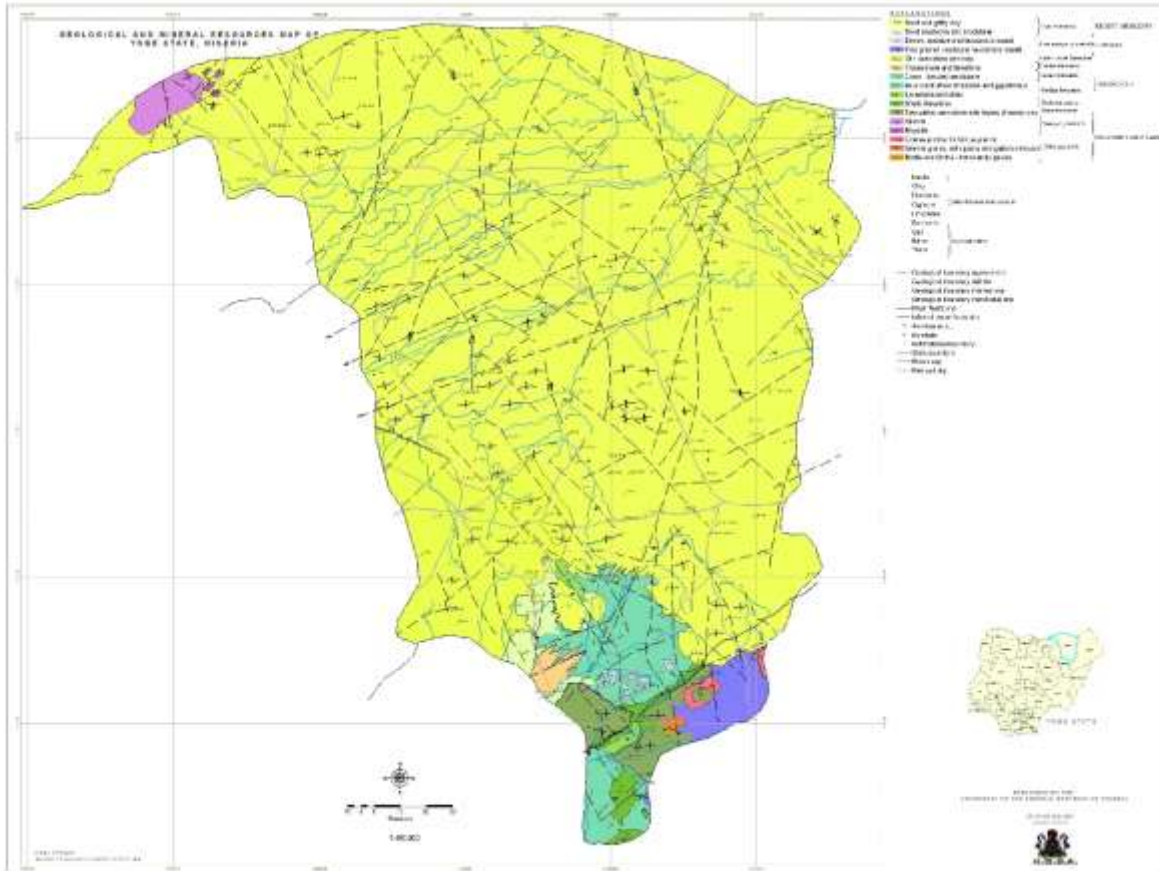
Integrates of aeromagnetic and aero-radiometric data to delineate structures and hydrothermal alteration zones associated with Gold and Base metal Mineralization in Chitipa area, Northern Malawi, the work identified northwest area as a promising mineralization zone, emphasizing the need for further exploration efforts in this region. The aforementioned work indicates that aeromagnetic and aeroradiometric data are good instruments in mineral resource investigation.

Researchers, in their efforts to mitigate unguided mining activities, have conducted several researches using various geophysical methods. Aerial survey techniques are mostly deployed due to their large area coverage and fast data acquisition. Most recent researchers such as Chisambi, et al. (2023); Jamaluddeen et al. (2019); Akinlalu et al. (2021); Taofeeq (2021); Rahimi, Kargarabafghi, Shahid, & Afkhami, (2024); Ogah & Abubakar (2024) have investigated mineral potential zones at global, regional and local level.

Despite numerous investigations on Nigeria formations, systematic geophysical analyses particularly those based on aeromagnetic and aeroradiometric interpretation are still limited in the study area. To address this gap, a detailed evaluation was conducted on the Formation using aeromagnetic and aeroradiometric data obtained from the Nigerian geological survey agency. Conventional interpretation methods, including source parameter imaging, analytical signal, lineament analysis, potassium to thorium ratio, ternary map and analytical hierarchical process using multicriteria decision analysis process assessment, were applied to quantify regions with very high to high mineral potential. In this research, aeromagnetic and aeroradiometric data were analyzed in order to identify mineral potential zones using multicriteria decision analysis process around Gashua (Sheet 41).

Location and Geology of the Area

Gashua is a town in Yobe State, northeastern Nigeria, situated close to the convergence of Hadejia and Jama' are rivers in the Chad Basin. It is located at latitude 12^o 52' North and Longitude 11^o 2' East. The Chad consist of three water bearing horizons i.e. the upper, middle, and the lower zones. Lithologically, the upper zone is composed of layers of clayed grits, sands and sandy clay of varying thickness. It has a population of about 125, 000 according to 2006 national population census result. The climate is characterized by short wet season (June – September) and long dry season (October – May), with high temperatures of about 39^oC to 45^oC. During the raining season, temperatures fall to 25^oC with annual rainfall of about 500 to 1000 mm (Emeka, Oniku, & Meludu, 2020).



Gashua is located within the Chad basin. The Chad basin extends to five countries in Africa, namely, Chad, Nigeria, Cameroon, Central Africa Republic, and Niger. The Basin lies between latitudes 11⁰ N and 14⁰ N and longitude 9⁰ E and 14⁰ E, covering Borno State, parts of Yobe and Jigawa States in Nigeria. About ten percent of the Chad Basin lies in the Northeastern part of Nigeria. The Chad basin resulted from plate divergence along the West Africa continental margin. The various processes which led to the plate divergence started with regional thermal doming, volcanism, rifting, formation of oceanic crust, marine incursion and subsequent widening and deepening of young oceans. Sedimentation in the Chad basin started in Albian times, the basal sedimentary sequence is the Bima sandstone, which was deposited unconformably over the Precambrian crystalline basement rock. Deposition of the Bima sandstone continued up to the Cenomanian. The Turonian was characterized by extensive transgression during which the Gongila Formation was deposited as a transitional sea deposit. The Fika shale was deposited during the transgression which began in the Turonian and continued up to the Senonian period (Emeka et al., 2020). Towards the end of the Cretaceous, during the Maastrichtian time, an estuarine deltaic environment prevailed in the basin and the Gombe sandstone, shale and limestone were deposited (Emeka et al., 2020). The Keri-Keri Formation was deposited unconformably on the eroded surface of the Gombe sandstone in the Pleistocene (Emeka et al., 2020). An unconformable Pleistocene deposit of the Chad formation was deposited on the Keri-Keri Formation (Emeka et al., 2020). The Keri-Keri formation is Eocene in age (Emeka et al., 2020).

Background Theory

The Total Magnetic field Intensity (TMI) at a region (Lowrie, 2007) is given as

$$T = \mu_0 H(1 - k) \tag{1}$$

where H is the magnetic strength, k is magnetic susceptibility, and μ_0 is permeability

T is subjected to polynomial fitting using the polynomial P(x,y) equation (Telford, Geldart, & Sheriff, 1990)

$$P(x, y) = a + bx + cy \tag{2}$$

where a, b, and c are constant obtain from the fitting, x and y are geographic coordinates

In this analysis P(x,y) is taken as the Regional Magnetic Intensity (R) that is removed from T to obtain Residual Magnetic Intensity (RMI)

$$RMI = T - R \tag{3}$$

The residual grid data was subjected to RTE using equation 2.4 in order to eliminate the effect of magnetic inclination in regions with low latitude by centering the peaks of the magnetic anomalies to their source body.

$$L(\theta) = \frac{\sin(I) - i \cos(I) \cdot \cos(D - \theta)^2 \cdot x(-\cos^2(D - \theta))}{[\sin^2(I_a) + \cos^2(I_a) \cdot \cos^2(D - \theta)] \cdot x[\sin^2(I) + \cos^2(I) \cdot \cos^2(D - \theta)]} \tag{4}$$

where I is geomagnetic Inclination, D is Geomagnetic Declination, I_a is Inclination for amplitude correction.

Developed by Telford, Geldart, & Sheriff, (1990) the SPI method is used to calculate depth (D) for fresh basement complex rock (Ezeh, Egwuonwu, Amadansun, & Umego, 2021) is given by

$$D = \frac{1}{\sqrt{\frac{\frac{\partial^2 T}{\partial^2 x} + \frac{\partial^2 T}{\partial^2 y}}{\frac{\partial^2 T}{\partial^2 x} + \frac{\partial^2 T}{\partial^2 y}}}} \tag{5}$$

The tilt angle (Telford, Geldart, & Sheriff, 1990) is given by

$$\theta = \arctan \frac{\frac{\partial T}{\partial x}}{\sqrt{\frac{\frac{\partial^2 T}{\partial^2 x} + \frac{\partial^2 T}{\partial^2 y}}{\frac{\partial^2 T}{\partial^2 x} + \frac{\partial^2 T}{\partial^2 y}}}} \tag{6}$$

Equation 7 give the relation of calculation Lineament Density (LD)

$$LD = \text{Length per unit Area} = \frac{l}{A} \tag{7}$$

2.1.1 Analytic Hierarchy Process (AHP)

The pairwise comparison between a set of criteria help make multifaceted decision (Saaty, 1990). First the thorny decision-making procedure between primary parameters is transformed in to a single level by pairwise comparison matrix in equation (8) (Saaty, 1977; Saaty, 1990)

$$A = \begin{bmatrix} a_{2i} & \dots & a_{2n} \\ \vdots & & \vdots \\ a_{n1} & \dots & a_{nn} \end{bmatrix} \quad (8)$$

In this judgement matrix, the elements are; $a_{2i} \dots \dots \dots a_{nn}$. The geometric average of the criteria is expressed in equation 8 (Saaty, 1977; Saaty, 1990)

$$W_n = \frac{G_i}{\sum_{i=1}^n G_i} \quad (9)$$

G_i and W_n respectively represent the geometric average and eigenvalue of the judgement of the i th row. The consistency of the normalized criteria weight is assessed using equation (9)

$$CR = \frac{CI}{RI} \quad (10)$$

Where CR is the consistency ratio, CI is the consistency index and RI is the consistency ratio index. For a normalized weight to be deemed consistent, the consistency ratio CR should be lower than 0.10 (Saaty, 1977; Saaty, 1990)

The consistency index CI is expressed in equation 11 as

$$CI = \frac{\lambda_{max} - n}{n - 1} \quad (11)$$

λ_{max} derived from equation 2.12 is the maximum eigenvalue of the judgement matrix

$$\lambda_{max} = \frac{1}{n} \sum_{i=1}^n \frac{(A_w)_i}{W_i} \quad (12)$$

The Groundwater Potential Zone (GWPZ) is calculated using equation (13)

$$GWPZ = \sum_i^n (x_i \times y_i) \quad (13)$$

where x_i is the weight of each thematic layer, y_i is the corresponding thematic or raster layer, i and n is the number of thematic layers

MATERIAL AND METHODS

Aeromagnetic and Aeroradiometric datasheets of Gashua (sheet 41) were acquired from Nigerian Geological Survey Agency (NGSA). A high resolution airborne geophysical survey involving magnetic and radiometric survey were carried out by Nigerian Geology Survey Agency with the help of Furgo Airborne Survey Limited, Johannesburg from 2004 to 2009 covering the entire country with the aim of developing geologic map of mineral resources of the country. Details of the survey equipment and flight specification is given in Table 1.

Table 1: Survey Equipment and Flight Parameters (Nigerian Geological Survey Agency, 2007)

Data sensors on board	Airborne magnetic gradient and GR320-3 (NaI) Multichannel radiometric gamma-ray spectrometer
Flight line spacing	500 m
Terrain clearance	80 m
Flight direction	NW – SE
Tie line spacing	2000 m
Tie line direction	NE – SW

Multicriteria Decision Analysis (MCDA)

Adopted in this research work is the AHP using Multi-criteria Decision Analysis (MDCA), the pairwise matrix was generated using factor (criteria scale) SPI, AS, Lineament Density, TC, and K/Th Ratio. An expert opinion established by (Saaty, 1977) shown in Table 3.3 was adopted in the research. Using the factors listed a pairwise matrix was generated in accordance with their importance over one another as shown in Table 2

Table 3.3: Expert Opinion (Saaty, 1977)

AHP Scale of Importance for Comparison of Pair	Numeric Rating	Reciprocal
Extremely Importance	9	1/9
Very Strong to Extremely Importance	8	1/8
Strongly to Very Strong Importance	7	1/7
Strongly to Very Strong Importance	6	1/6
Strong Importance	5	1/5
Moderately to Strong Importance	4	1/4
Moderate Importance	3	1/3
Equally to Moderate Importance	2	1/2
Equal Importance	1	1

Table 3.4: Pairwise Matrix

Factor	SPI	MLD	ELD	LID	E	SL
SPI	1.00	5.00	3.00	7.00	9.00	7.00
MLD	0.20	1.00	5.00	5.00	9.00	5.00
ELD	0.20	0.20	1.00	0.33	0.50	5.00
LID	0.20	0.20	3.00	1.00	9.00	3.00
E	0.20	0.20	3.00	0.11	1.00	3.00
SL	0.20	0.20	3.00	1.00	0.33	1.00
SUM	2.00	6.80	18.00	14.44	28.50	24.00

SPI=Source Parameter Imaging, MLD=Magnetic Lineament Density, ELD=Elevation Lineament Density, E=Elevation, SL=Slope

Table 3.5: Normalized Pairwise Matrix showing the Weight, Consistency index, Random Consistency index and Consistency Ratio

Normalization	SPI	MLD	ELD	LID	E	SL	Average	Lamda	CI	RCI	CR
SPI	0.50	0.74	0.17	0.48	0.32	0.29	0.42	9.21	0.13	1.24	0.10
MLD	0.10	0.15	0.28	0.35	0.32	0.21	0.24	9.33			
ELD	0.10	0.03	0.06	0.02	0.02	0.21	0.05	4.01			
LID	0.10	0.03	0.17	0.07	0.32	0.13	0.14	9.09			
E	0.10	0.03	0.17	0.01	0.04	0.13	0.07	8.49			
SL	0.10	0.03	0.17	0.07	0.01	0.04	0.08	6.63			
SUM	1.00	1.00	1.00	1.00	1.01	1.00	1.00	9.21			

Table 3.6: Saaty's random index (RI) for different values of n

N	1	2	3	4	5	6	7	8	9	10
RI	0.00	0.00	0.52	0.90	1.12	1.24	1.32	1.41	1.45	1.45

The pairwise matrix comparison was normalized using equation (2.8) as shown in Table 3.2, Table 3.6 show Random Index (RI) given in (Nazaripour, Sedaghat, Shafaie, & Rad, 2024) used to calculate the Consistency Index (CI). The Consistency Ratio (CR), Consistency Index (CI) and maximum eigenvalues of the judgement matrix shown in Table 3.5 were calculated using equation (2.9), (2.10) and (2.11). The groundwater Potential Map (GWPM) was generated by multiplying thematic layers with it respective weighted values, the products were sum up using raster calculator menu in ArcGIS Environment (equation (2.13)).

Interpretation

Total Magnetic Intensity (TMI)

The total magnetic intensity map shows variation in magnetic intensity spread across the area. High magnetic anomalies of value range of 33020.6nT to 33117.5nT were observed in the NE, NW, SW and SE, intermediate to low intensity anomalies were observed to be predominantly in the NE, NW and SW regions with values ranging from 32697.9nT to 33015.5nT.

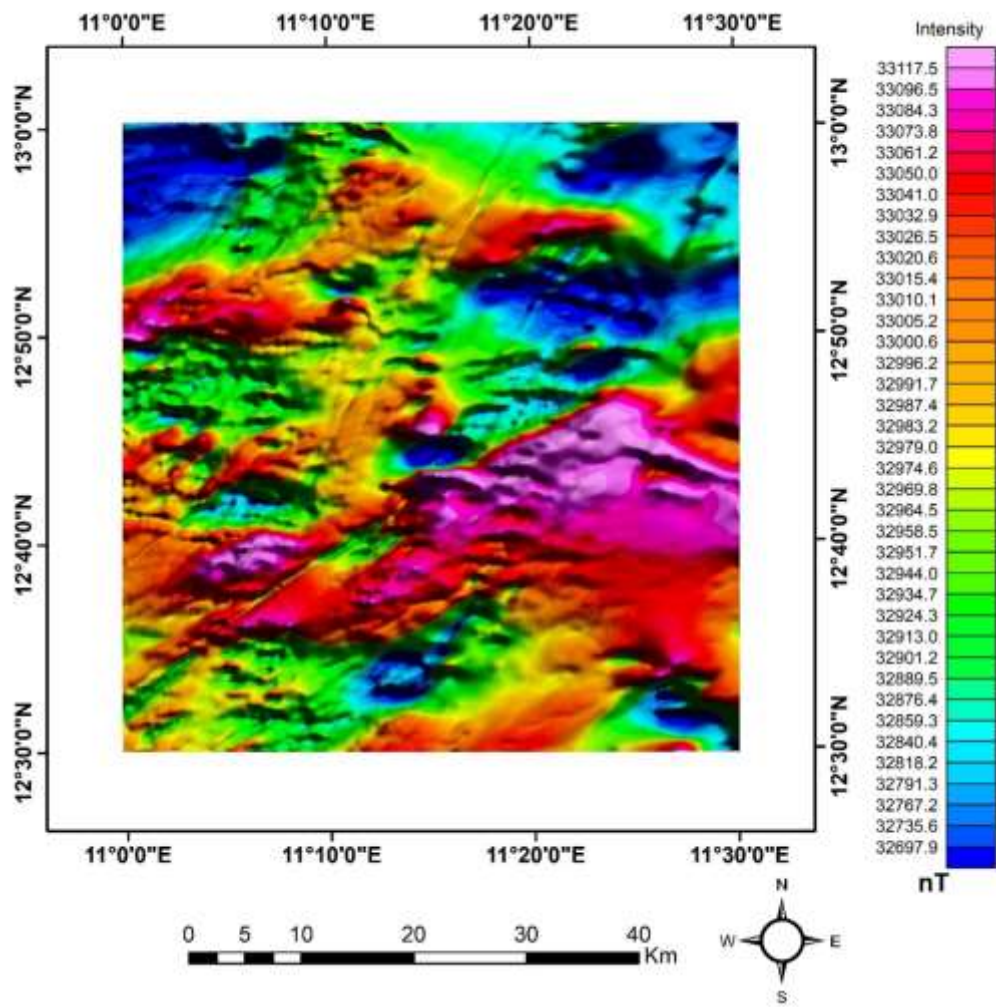


Figure 1: TMI Map of the Study Area

Figure 3 shows regional maps of the study area. It was observed that the regional field trend pattern is NE-SW.

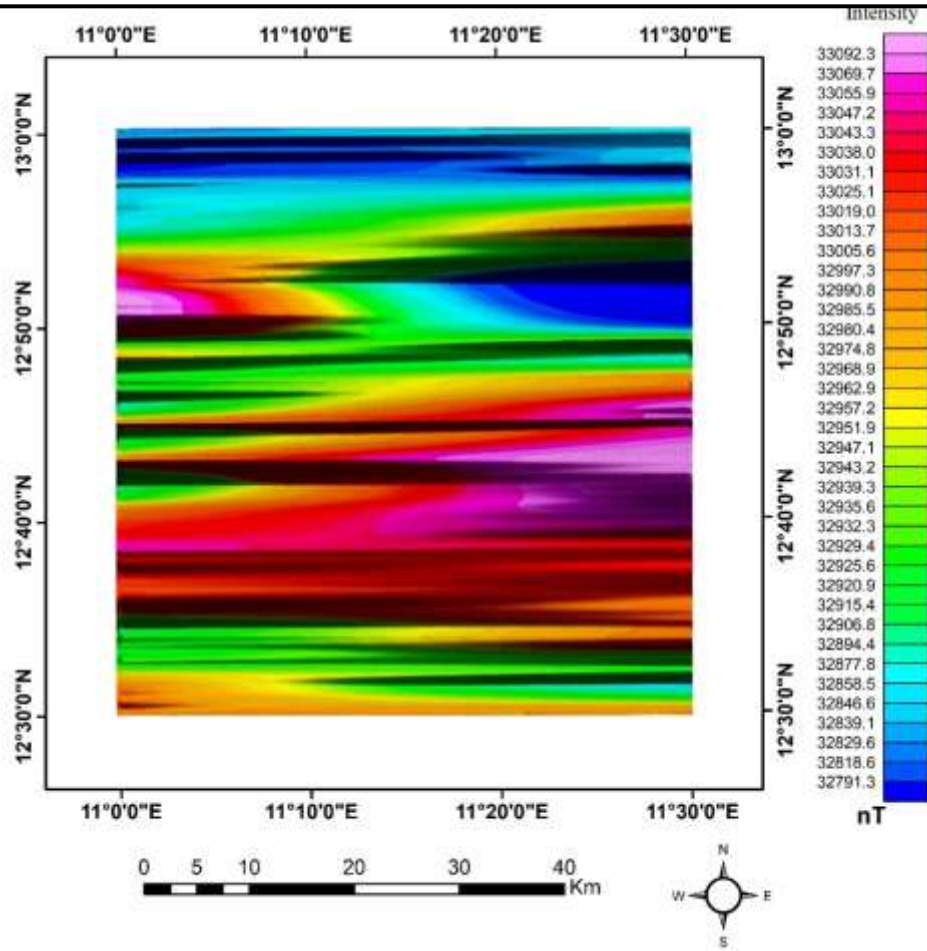


Figure 2: Regional Map of the Study Area

Figure 4 shows the residual map of the study area and was produced after the removal of regional data from the total magnetic field data. It shows region of high, intermediate and low magnetic intensity within the study area. The anomalous trend of the area trends NE-SW indicating the direction of subsurface lineaments controlling the geologic activities.

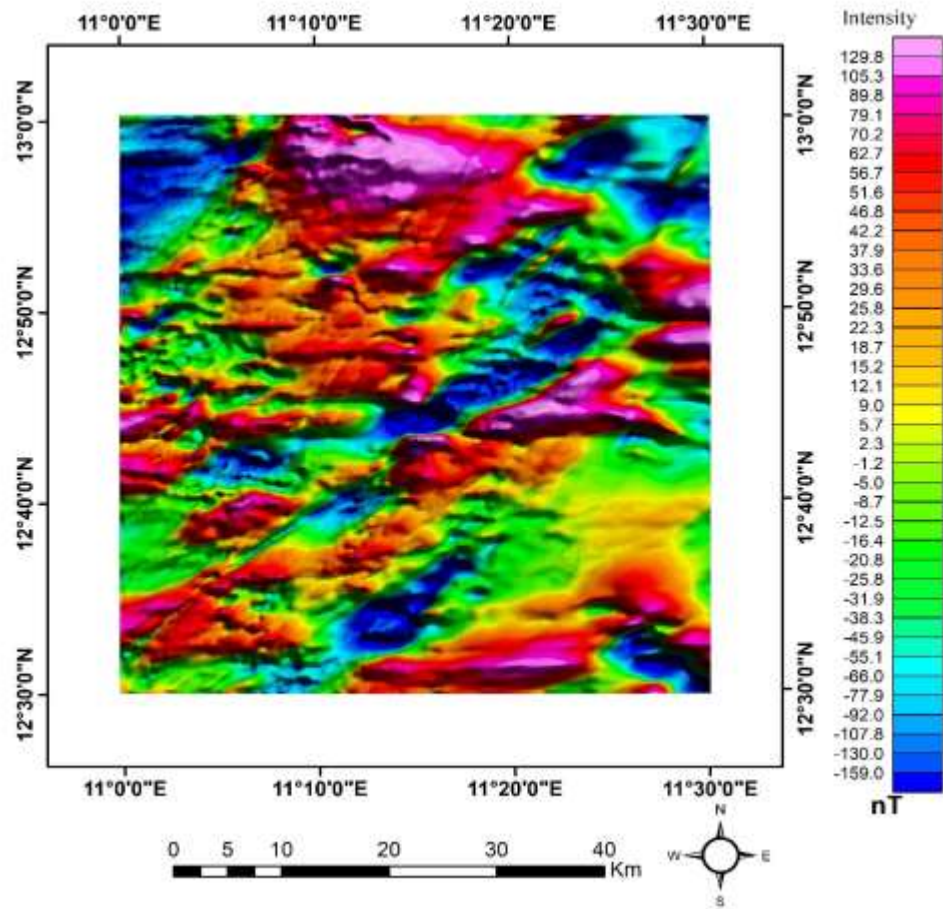


Figure 3: Residual Map of the Study Area

Figure 5 shows reduction to the equator (RTE) map of the study area. This map shows a striking resemblance to the TMI and residual map of the area with high magnetic anomalies in the NE, NW, SW and SE. Low to intermediate magnetic anomalies were noticed in the NE, NW, SW and SE of the area.

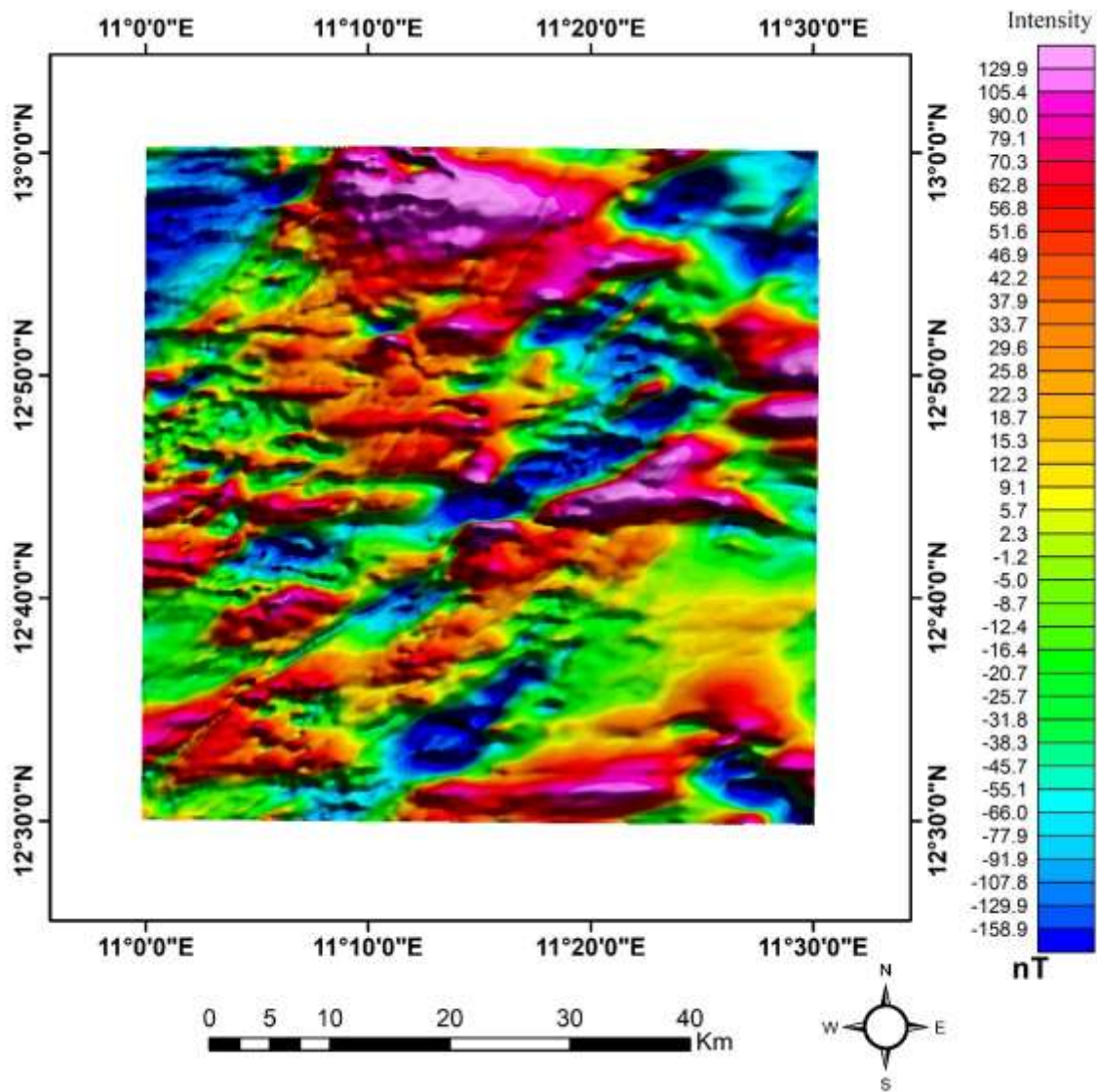


Figure 4: RTE Map of the Study Area

The results obtained after applying the FVD filtering method (Figure 6) provides a good representation of features closer to the subsurface, e.g., faults (red lines). most of the area is covered by high-frequency anomalies, inferred shallow depth to causative sources in comparison with some other parts such as southeast, northeast, and part of north central with deeper sources which have the presence of sedimentary covers. Also, on the map are long and short linear features (red and blue lines) distinguishing the edges of magnetic source bodies with zero contour lines representing the locations of the contacts or faults.

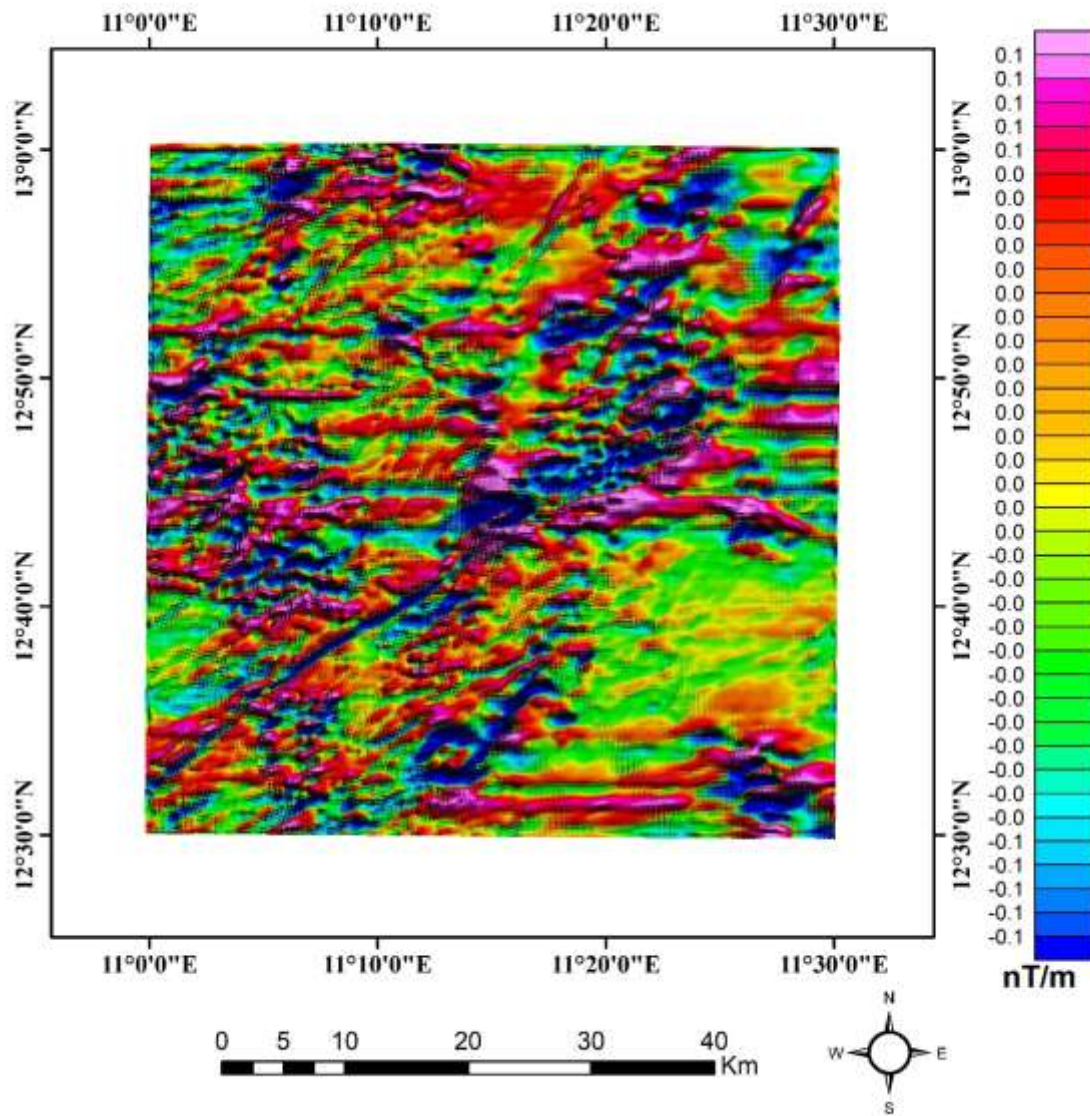


Figure 5: FVD Map of the Study Area

The CET grid analysis was applied to the RTE map in order to identify linear structures. It is observed that the majority of the prominent structural features in Figure 8 are trending NE–SW while fewer ones are trending in the NW–SE, E–W, and N–S directions. These trends reveal the effects of the deep heterogeneity of the Earth’s crust which represents fractures–faults affecting the overlying sediments. The orientation of these deduced lineaments is plotted using a rose diagram (Figure 8).

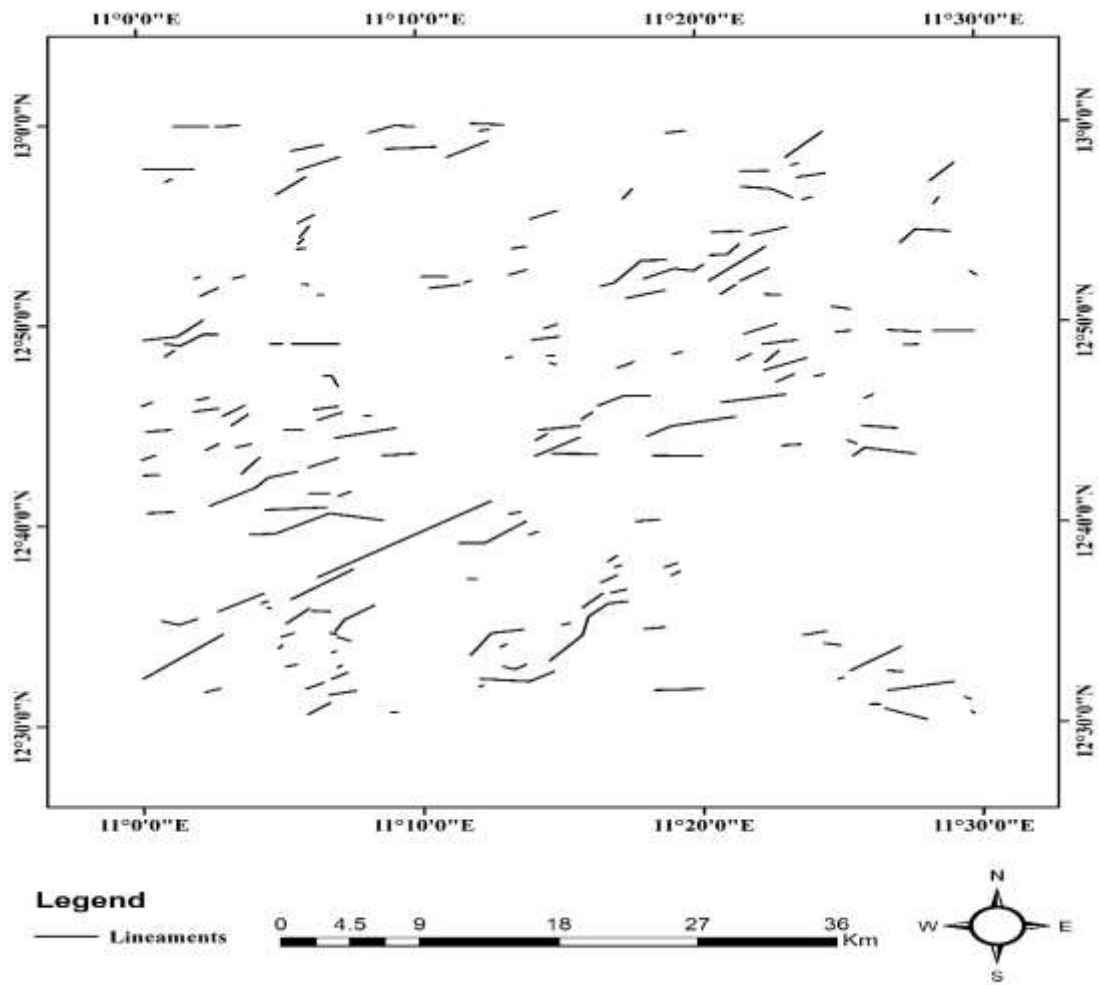


Figure 6: Lineament Map of the Study Area

Figure 7 shows an SPI map of the study area. This map indicates regions with deeper, intermediate and shallow depths.

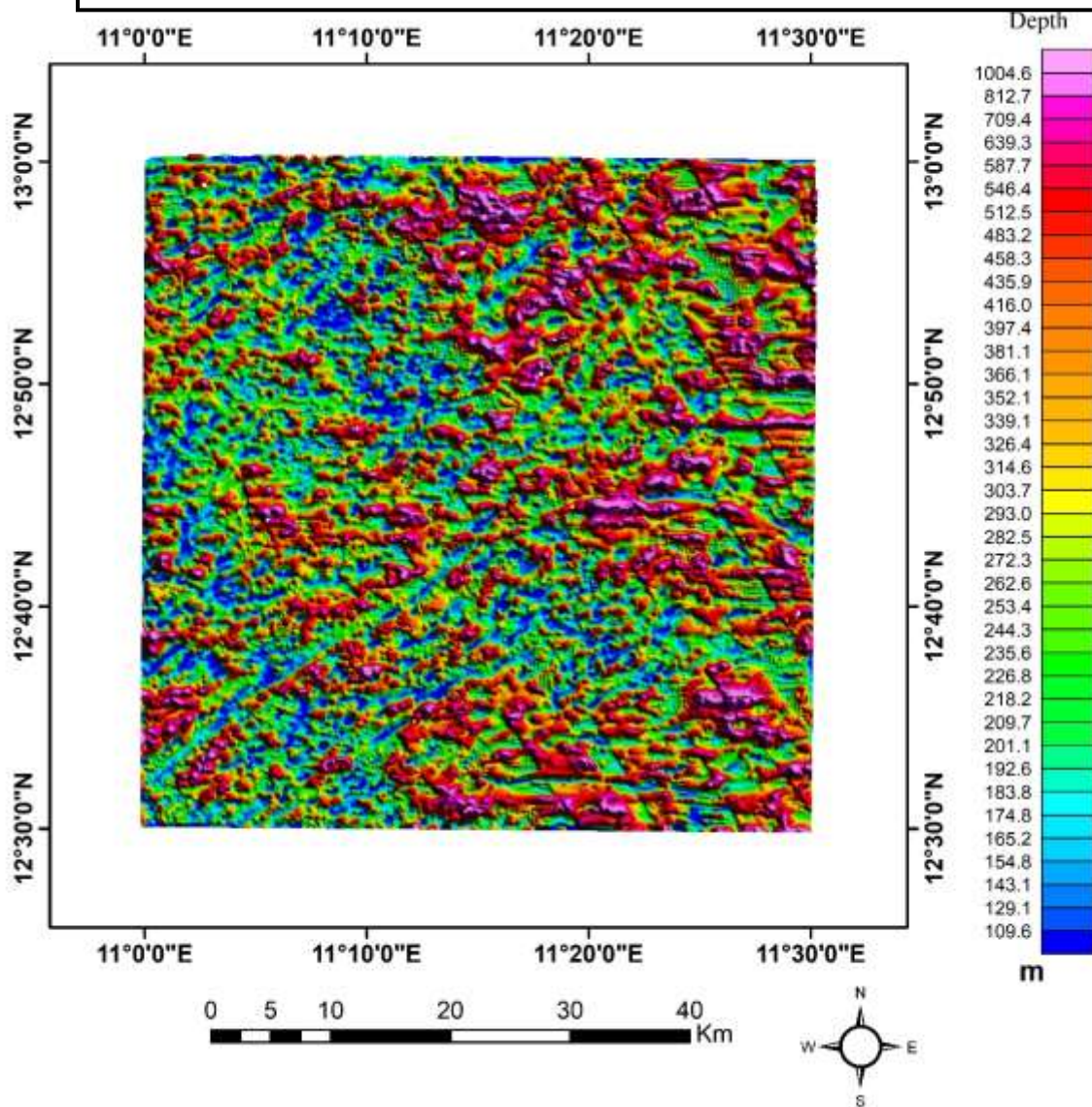


Figure 7: SPI Map of the Study Area

The deeper Analytical Signal (AS) map shown in Figure 8 indicates three magnetic domains: (i) a domain of gradient maxima (gradient between 0.059 and 0.234 nT/m) which can be regarded as outlines of magnetic sources some of these maxima are noticeable in the NE, NW, and SW regions of the area; (ii) a domain of intermediate intensities with gradients ranging from 0.027 to 0.056 nT/m; and (iii) a domain of low intensities with gradients located between 0.009 and 0.024 nT/m. In the first magnetic domain, the majority of maxima are trending in the NE–SW direction.

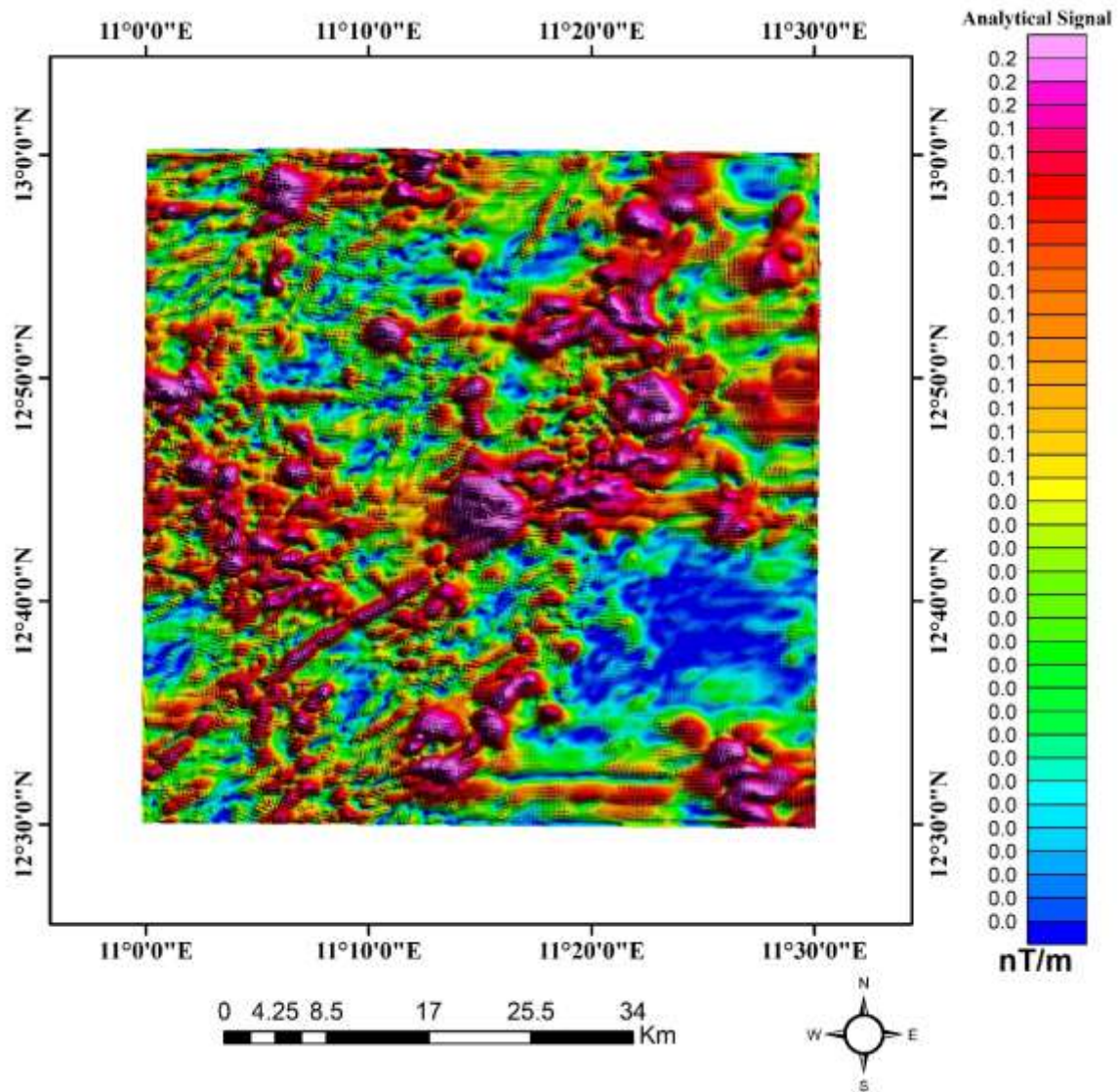


Figure 8: AS Map of the Study Area

Potassium percentage (K%) map, equivalent thorium (eTh ppm), equivalent uranium (eU ppm) and total count (TC) in $\mu\text{R/h}$ were interpreted. High % of K were observed to trend in NE to NW direction, and in the SW region of the area with value range of 1.0% to 1.5% as indicated in figure 9. Low to intermediate percentage were observed in the SE and NW region with value range of 0.4% to 0.9%.

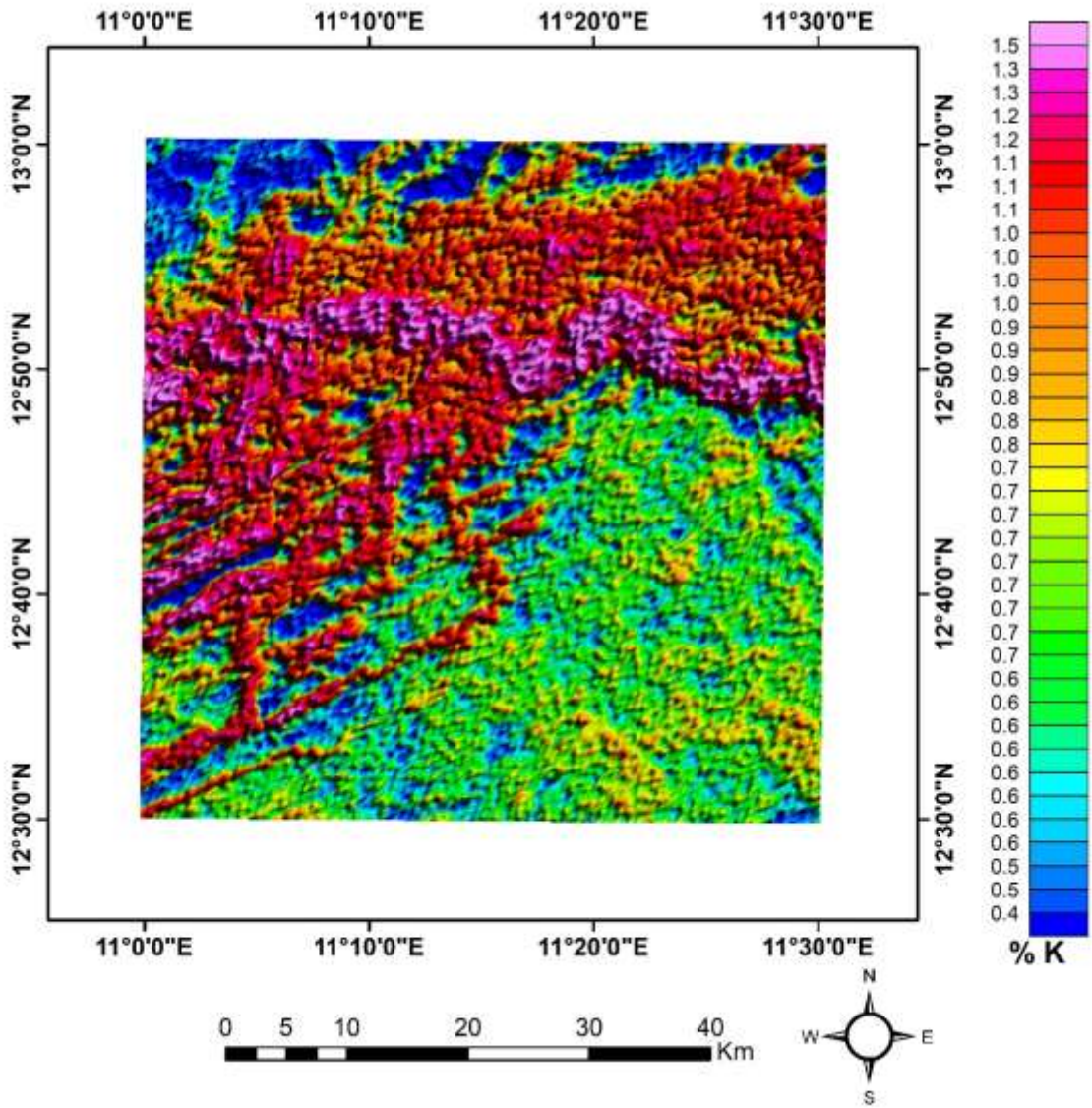


Figure 9: %K Map of the Study Area

eTh in Figure 10 shows high eTh content in the NE, NW and SW region of the area with value range of 10.1ppm to 15.4ppm. low to intermediate value range of 4.4ppm to 9.8ppm were observed in the SE, SW and NW regions of the area.

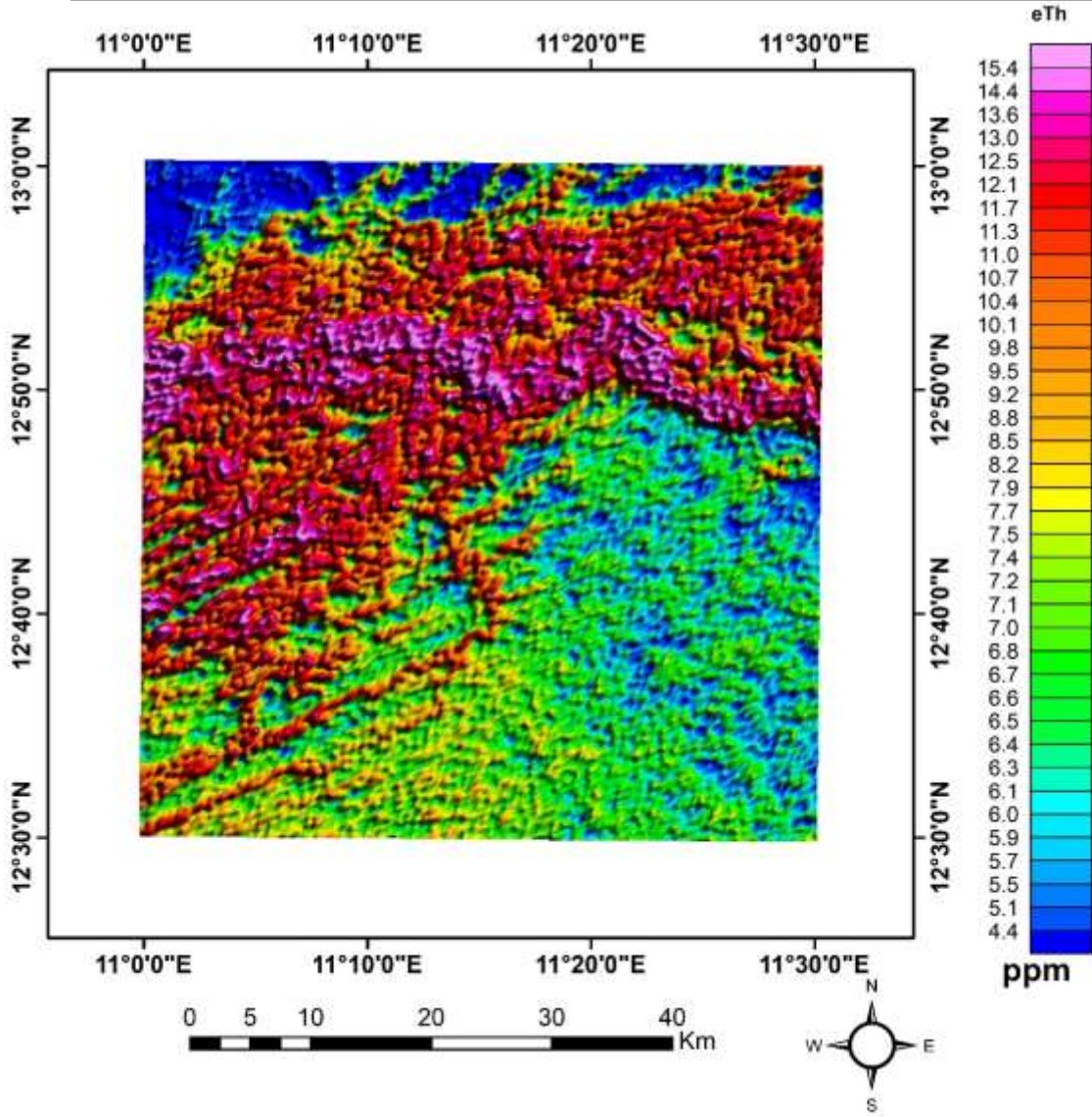


Figure 10: eTh Map of the Study Area

The eU map in Figure 11 shows low - to - intermediate values of 0.0ppm to 1.5ppm and high concentration in the NE, NW and SW regions with value range of 1.6ppm to 3.1ppm.

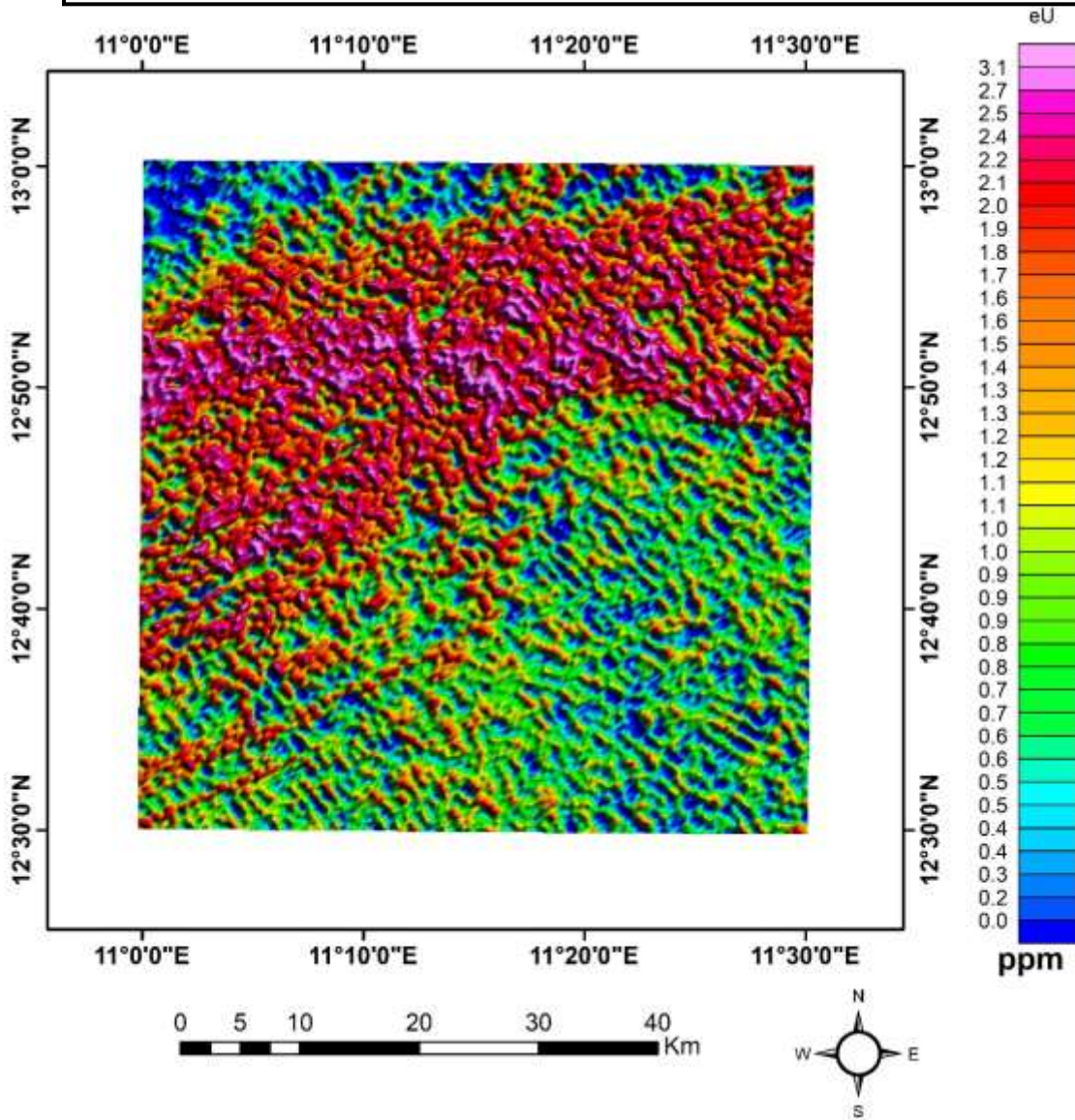


Figure 11: eU Map of the Study Area

The TC map in Figure 12 shows high concentration level in the NE, NW and SW zones with value range of 1537.4 μ R/h to 2215.6 μ R/h.

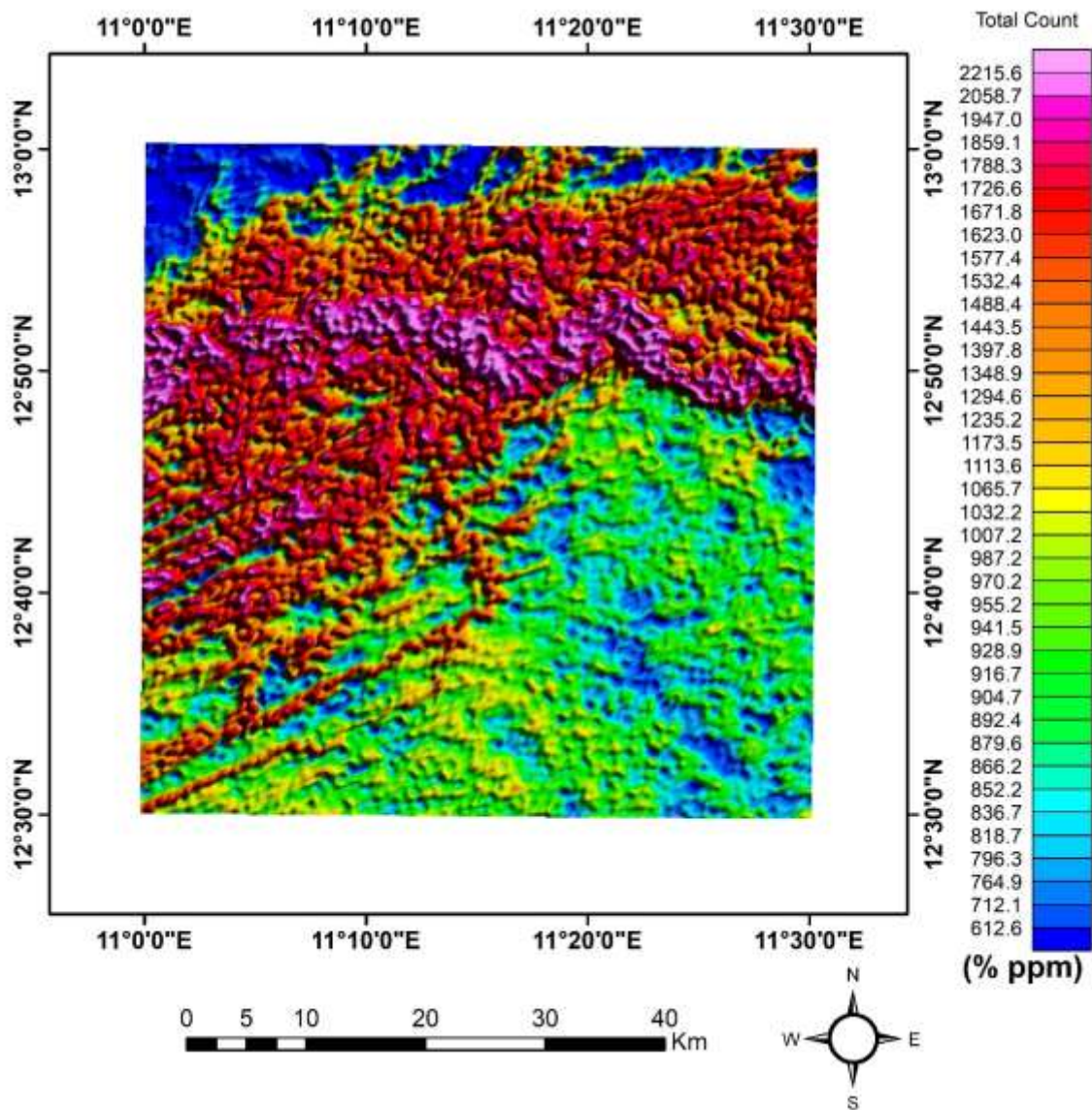


Figure 12: TC Map of the Study Area

Finally, the ternary map (Figure 13) of the study area was generated by modulating the three colors red (R), green (G), and blue (B) in equal proportion so that their intensities could be revealed. From this map, the lithological contrasts resulting from geological and mineral explorations can be interpreted. Here the white color found in some areas across the study area shows the high level of concentration for the radioactive elements which is characterized by strong radiometric response, and these areas can be associated with metasediments, younger granite, schist felsites, and metamorphic rocks. The low concentration of the radioactive elements that represented black is a resultant of metavolcanic and metagabbro rocks. The red color represents high K content, but low Th and U related to metasedimentary rocks, while the green color corresponds to regions of high Th, low K, and U associated with metavolcanic rock formations in the study area.

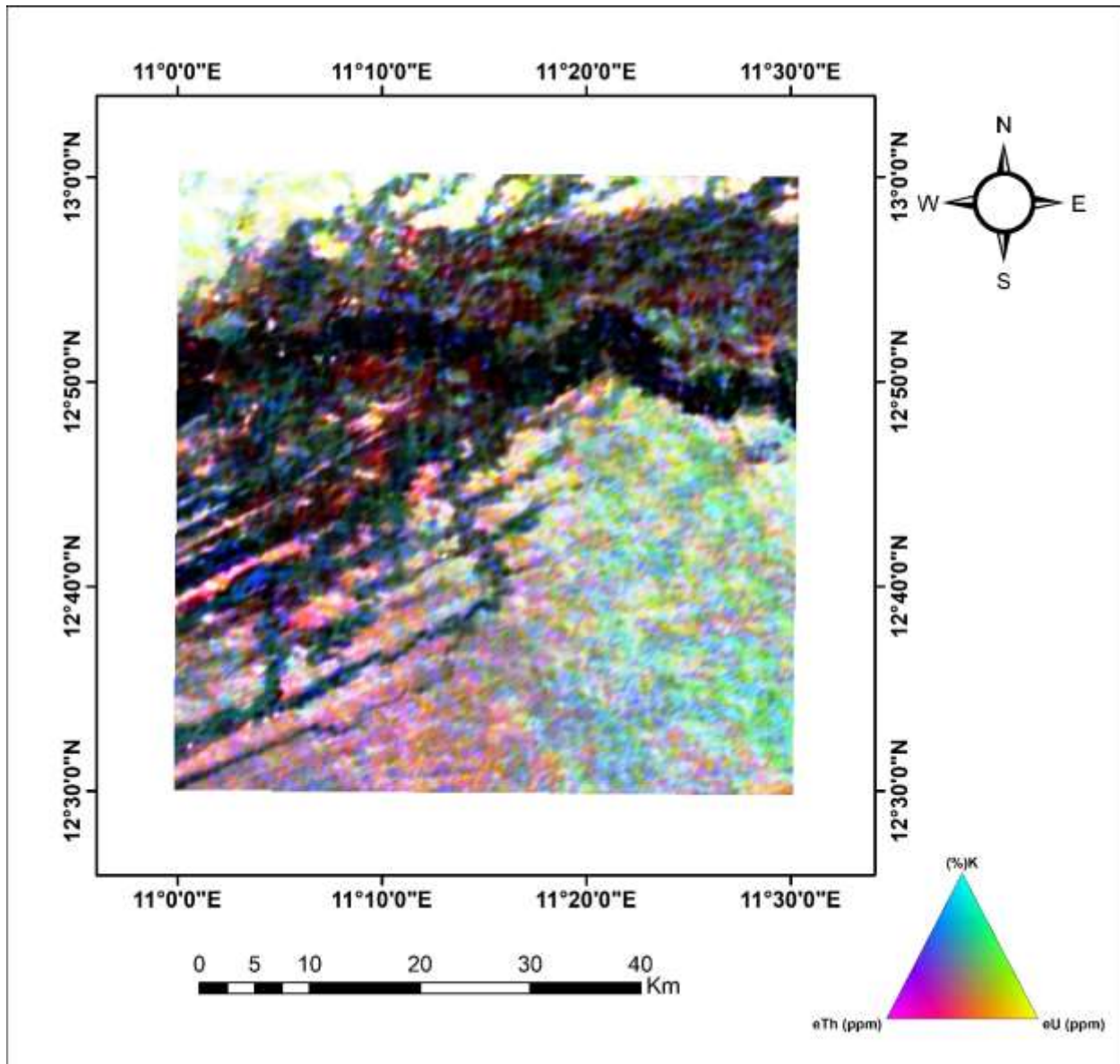


Figure 13: Ternary Map of the Study Area

K/Th ratio map in Figure 14 shows high hydrothermal alteration zones of values ranging from 0.107%ppm to 0.130%ppm predominantly in the SE and NW region with fewer locations in the NE and SW region. Low to medium hydrothermal alteration zone of value range of 0.066%ppm to 0.106%ppm were observed in the NE, SW and NW region of the area. These regions with high alteration are good indication of mineralisation zones.

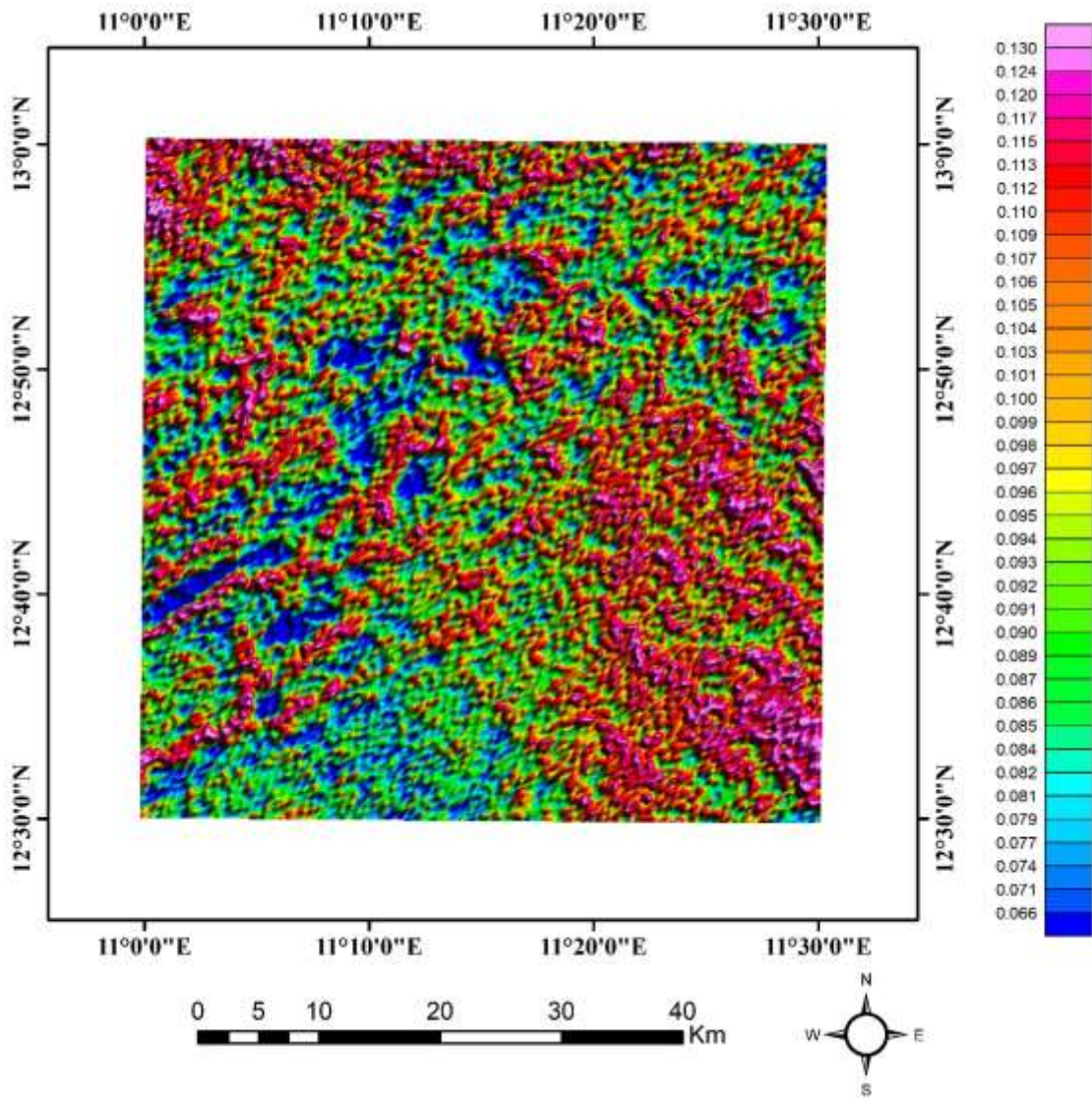


Figure 14: K/Th Ratio Map of the Study Area

Thematic Layers

Five thematic layers were generated from the SPI, AS, lineament density, TC, and K/Th ratio grids as in Figure 15, 16, 17, 18 and 19. The thematic layers were resampled and reclassified in to five classes; very high, high, moderate, low and very low

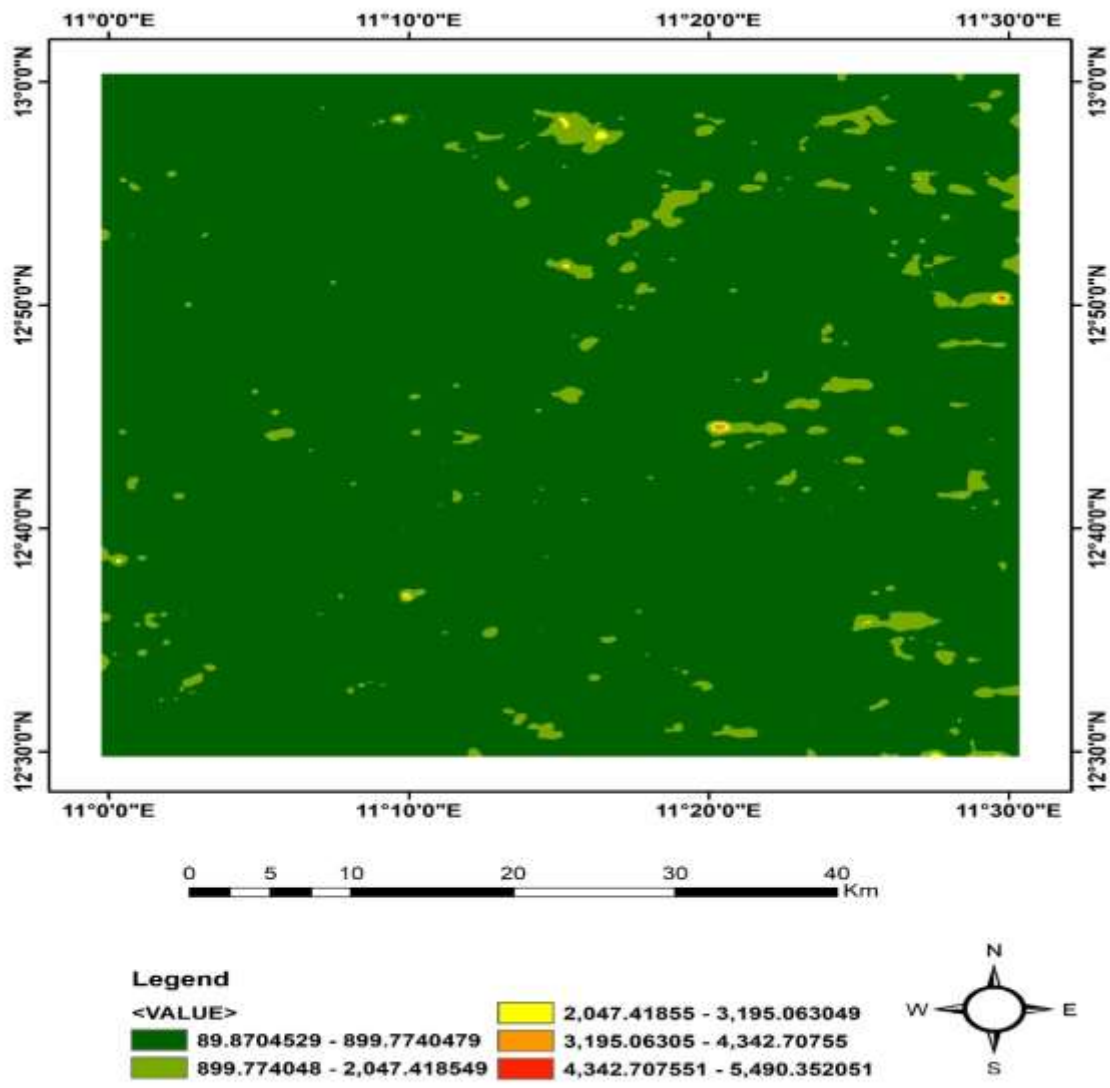


Figure 15: SPI Reclassified Map

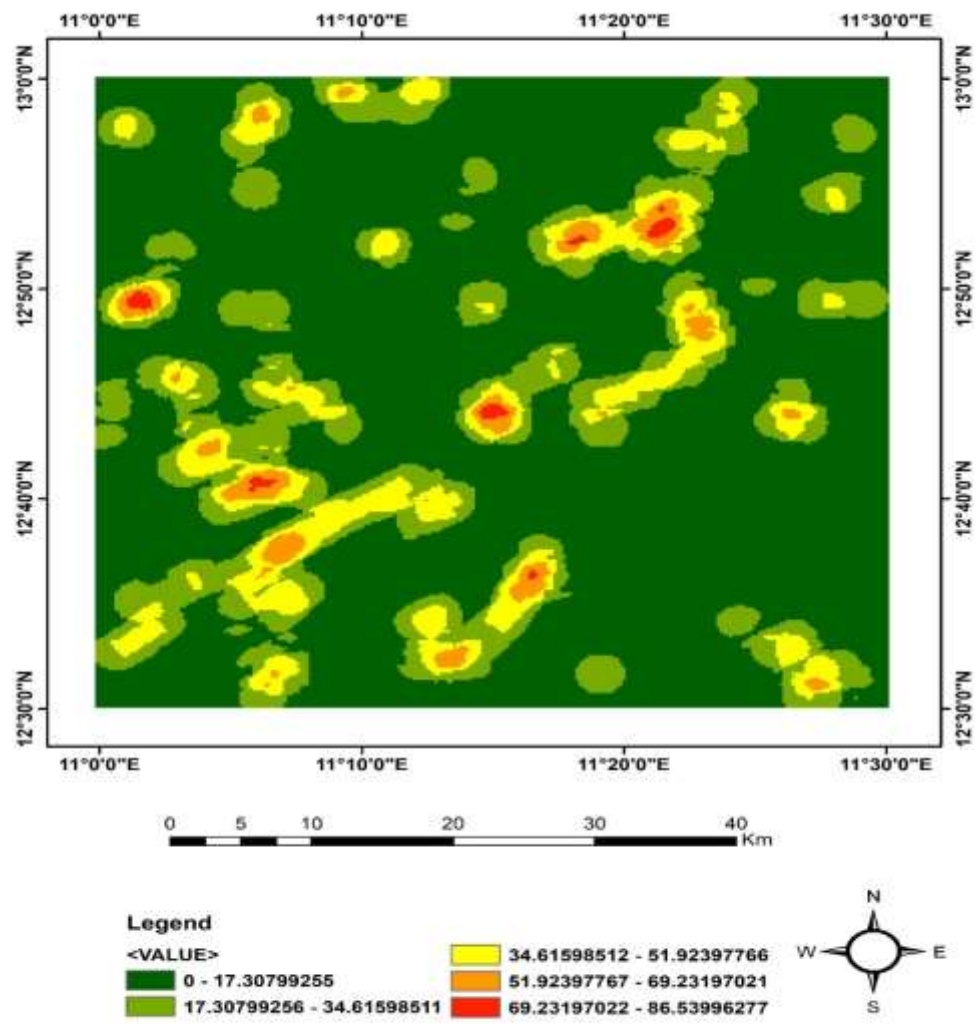


Figure 16: Lineaments Density Reclassified

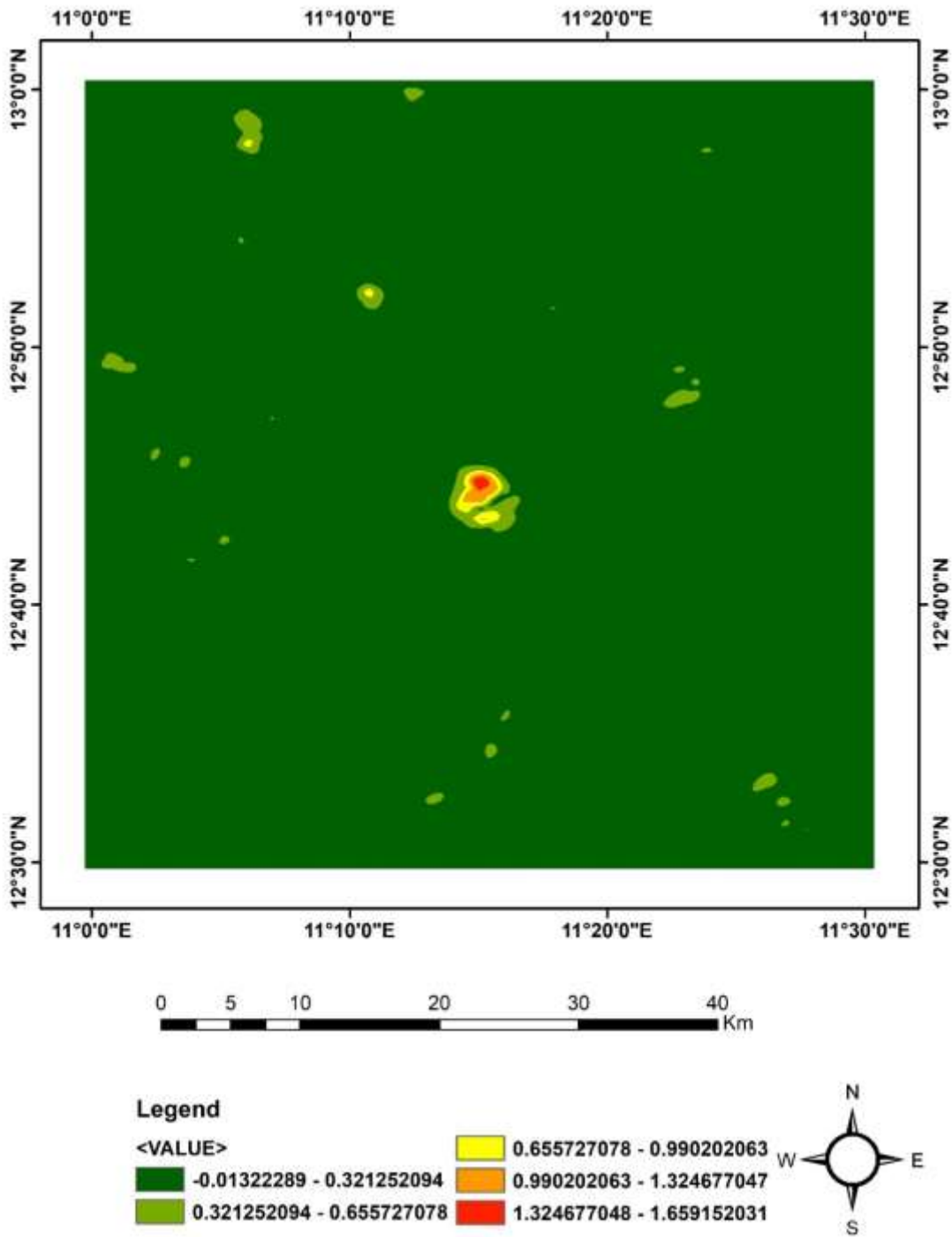


Figure 16: AS Reclassified Map

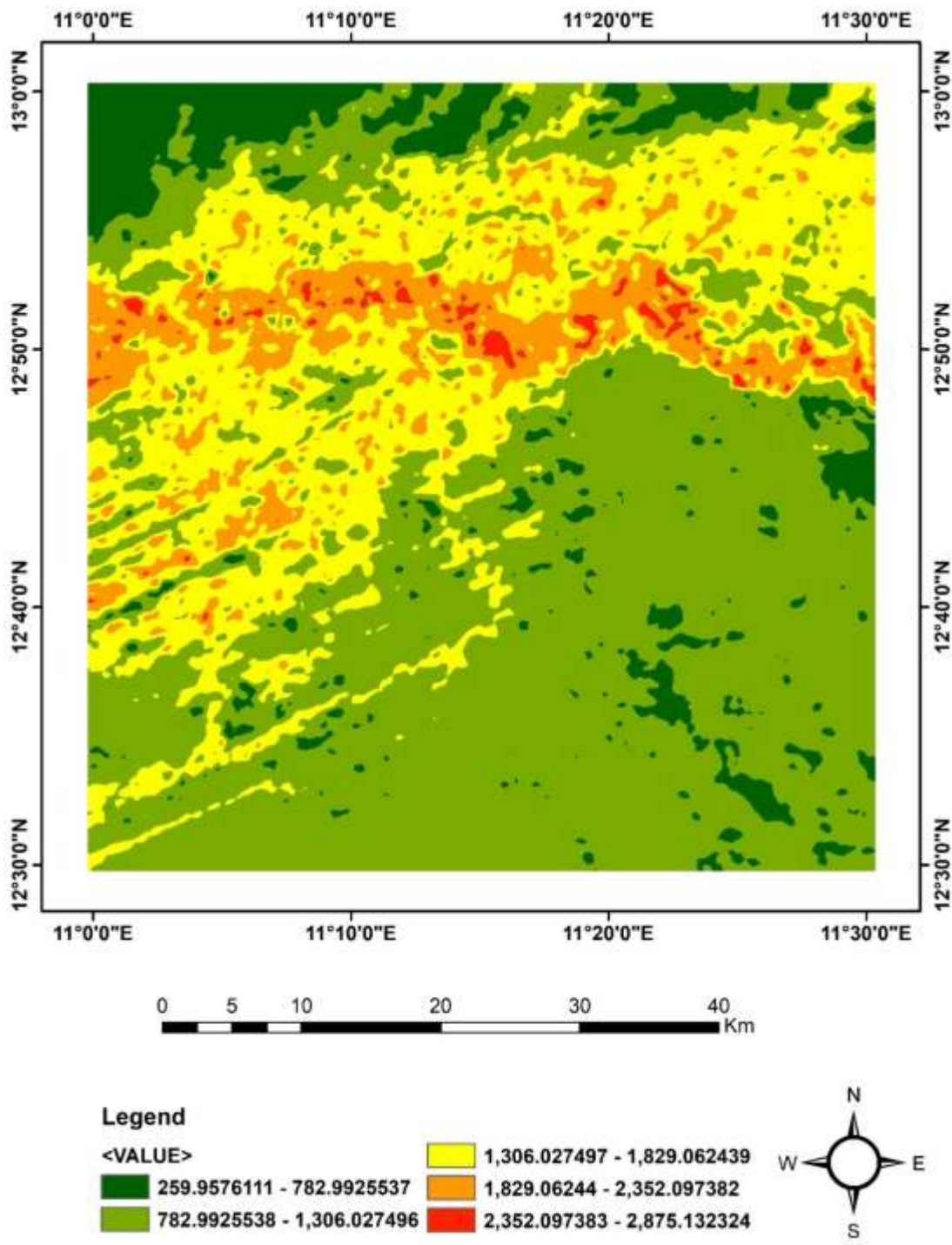


Figure 17: TC Reclassified Map

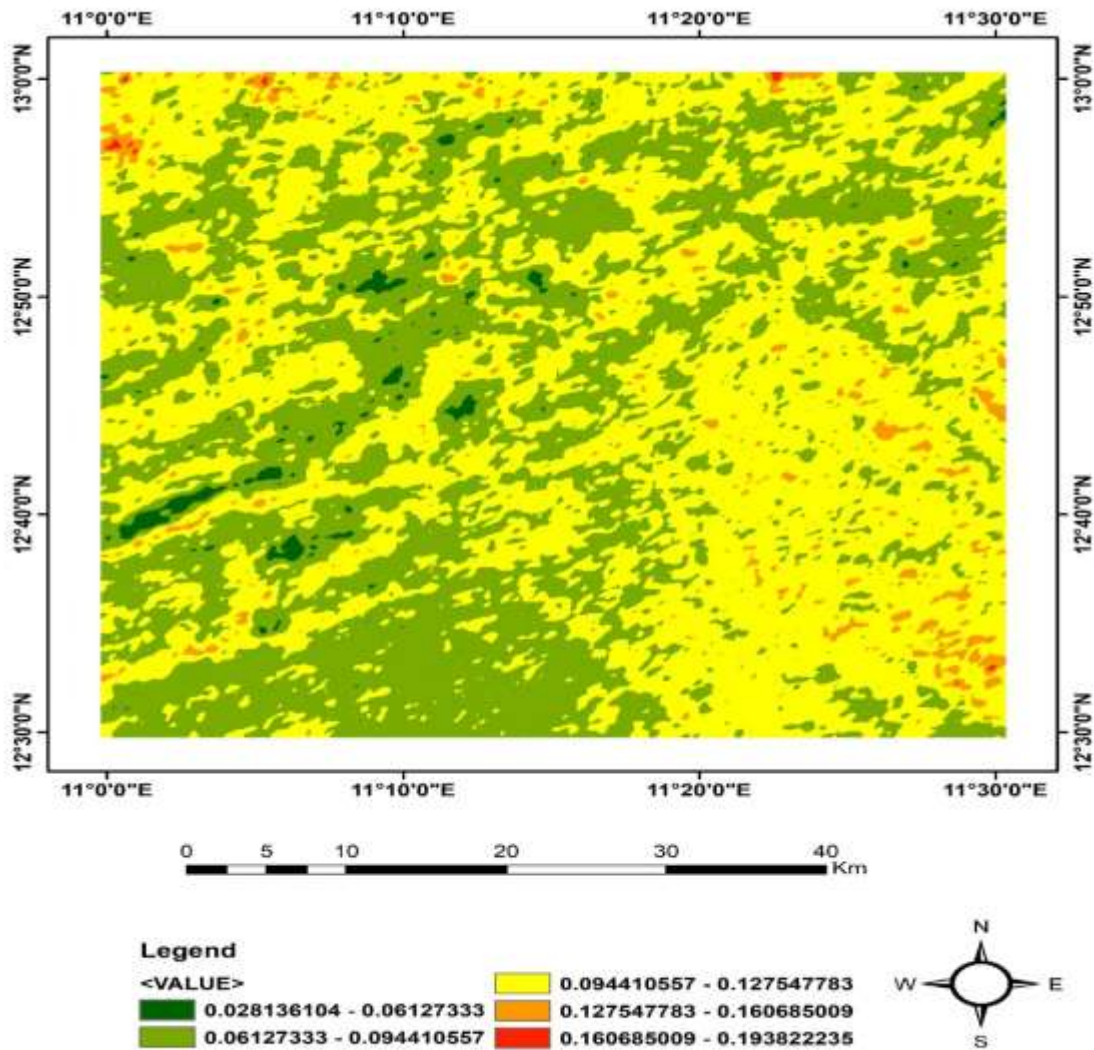


Figure 18: K/Th Ratio Reclassified Map

The SPI layer (Figure 15) shows moderate depth around NE and SE region of the area with shallow depth covering most of the area. The lineament density layer (figure 16) shows the area to have very high to moderate lineament density trending in the NE to SW direction. Very low lineament were also observed in the NE, NW, SW and SE region of the area. The AS layer (Figure 17) shows very high to moderate domain gradient signal around the center of the study area and small area of moderate domain gradient signal in the NW and SE regions of the study area, it was observed that the area is mostly covered by very low domain gradient signals. The TC layer (Figure 18) shows very high to moderate concentration count to trends from NE to NW part of the area through SW area. Very low to low count were observed in the SE and NW regions of the area. K/Th ratio layer (Figure 19) was observed to have very high hydrothermal alteration zones in the NE, SE and NW regions, moderate alteration zones were observed predominantly in the SE and NW regions of the study area. The regions with very high to moderate domain gradient signal and hydrothermal alteration zone are inferred as areas with mineral potential.

RESULTS AND DISCUSSIONS

The results of this research work is presented in graph (pseudo-section) and table.

Results

Figure 19 and Table – shows the mineralisation potential and the area coverage of the regions with very high, high and moderate mineral potential.

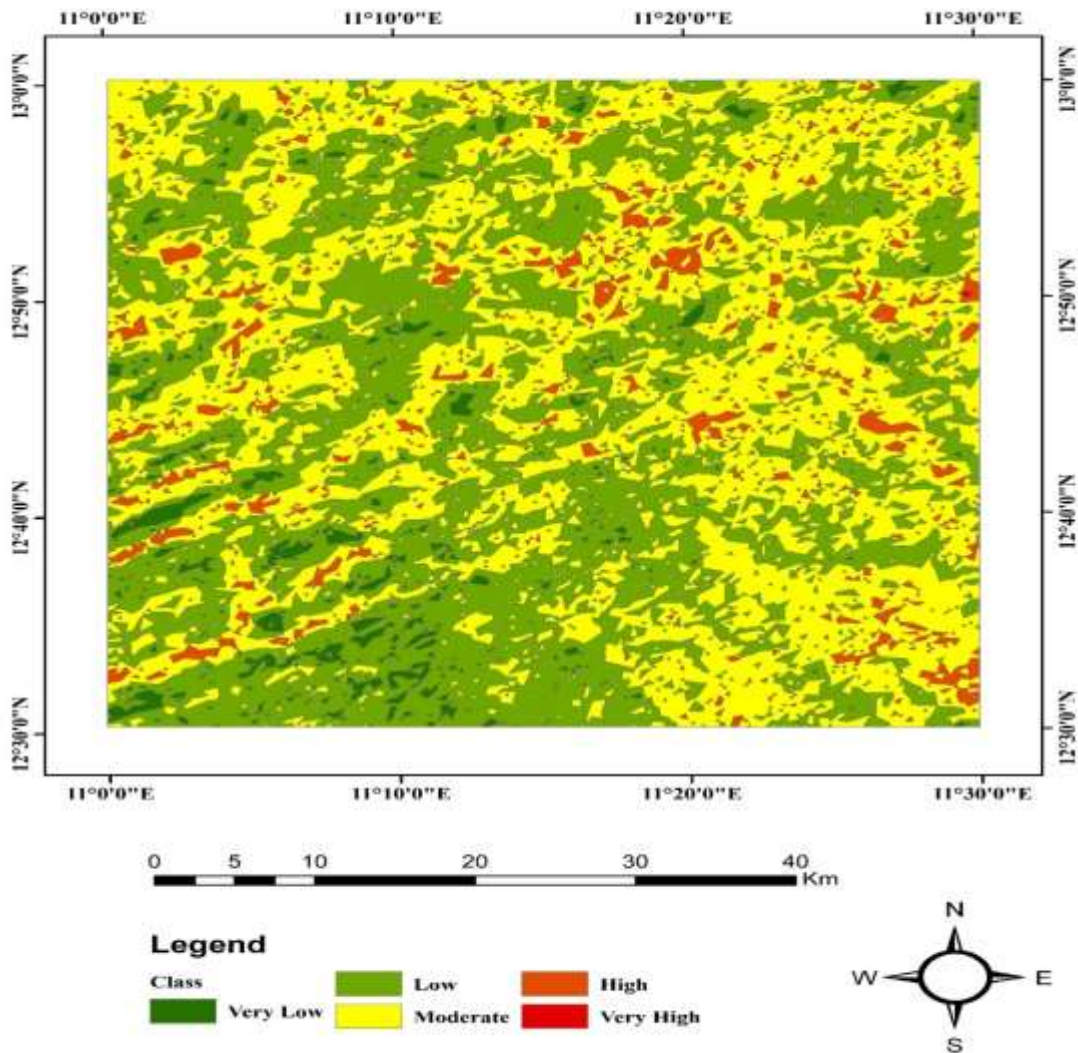


Figure 19: Mineral Potential Map of the Study Area

SN	Long	Lat	Area	Class
1	11 ^o 09'13.4318''	12 ^o 40'24.802''	82.634531	Very Low
2	11 ^o 13'42.0554''	12 ^o 44'04.125''	1353.336765	Low
3	11 ^o 16'20.4731''	12 ^o 46'07.547''	1450.891613	Moderate
4	11 ^o 16'10.4779''	12 ^o 45'58.671''	145.515644	High
5	11 ^o 29'37.8171''	12 ^o 50'10.236''	0.176701	Very High

Discussion

Aeromagnetic and aeroradiometric data were integrated using Multicriteria Decision Analysis (MCDA) to isolate potential mineralisation zones around Gashua and its environs, Northeastern Nigeria. The AS map (Figure 8) shows regions of high domain gradient and low domain gradient signals around the area. High domain gradient signals were observed at the center, NE, NW and SW region of the area with value > 0.1nT/m. these regions of high signals area inferred as regions of possible mineralisation potential. The CET analysis of the data shows lineaments which were inferred as areas of possible minerals accumulation zone, the lineaments were observed to trend in the NE to SW direction. K/Th ratio map (Figure 14) reveals the hydrothermal alteration zones of the area. High hydrothermal alteration zones with value >0.107%ppm were observed predominantly in the SE and NW region of the study area. Cross-correlating AS, lineaments, K/Th ratio maps, it was inferred that the mineralisation potential regions in this area are in the NW and SE regions. The MCDA results isolates areas with mineralisation potential in to very high, high, moderate, low and very low potential zones. Regions with very high mineral potential has an area coverage of 0.176701km², region of high mineral potential has an area coverage of 145.515644km², region of moderate mineral potential has an area coverage of 1450.891613km², region of low mineral potential has an area coverage of 1353.336765km², and region of very low mineral potential has an area coverage of 82.634531km². the results revealed that the area is mostly of moderate mineral potential.

CONCLUSION

Aeromagnetic and aeroradiometric data were deployed to isolate regions of mineralization potential. The study concludes that the area is of moderate mineralisation potential based on the fracturing, high domain gradient signal and hydrothermal alteration observed in the area. The study was able to classify the area into five class; very high, high, moderate, low and very low mineral potential with area coverage 0.176701km², 145.515644km², 1450.891613km², 1353.336765km² and 82.634531km² respectively. In conclusion, the area was observed to be of moderate potential. It is recommended that ground geophysical and geochemical ground be carried out in the area to acquire more information on the mineralization and mineral in the area.

REFERENCES

- Akinlalu, A., Olayanju, G., Adiat, K., & Omosuyi, G. (2021). Mineralisation potential assessment using analytical hierarchy process (AHP) modeling technique: A case study of Ilesha schist belt, southwestern Nigeria. *Results in Geophysical Sciences*, 1-17. doi:<https://doi.org/10.1016/j.ringps.2021.100026>
- Chisambi, J., Haundi, T., & Ghambi, S. (2023). Integrated interpretation of aeromagnetic and aeroradiometric data to delineate structures and hydrothermal alteration zones associated with Gold and Base metal Mineralization in Chitipa area, Northern Malawi. *International Journal of Mining and Geo-Engineering*, 305-313. doi:DOI: 10.22059/IJMGE.2023.354353.595027
- Emeka, A. L., Oniku, A. S., & Meludu, O. (2020). Evaluation of Groundwater Potential in Gashua Northeast Nigeria, Using Electrical Resistivity Method. *Communication in Physical Sciences*, 5(3), 281-290. Retrieved from <https://journalcps.com/index.php/volumes>

- Ezeh, O., Egwuonwu, G., Amadansun, C., & Umego, M. (2021). Source parameter imaging of aeromagnetic map of Sokoto Basin, Northwestern Nigeria. *Int. J. Mech. Civ. Eng.*, 1-11.
- Hussaini, A., Idi, B. Y., Ndikilar, C. E., Nasir, M. M., Alhassan, A., Bala, N., . . . Ayuba, I. (2021). Determination of Depth to Basement Using Spectral Analysis of Aeromagnetic Data over Azare Segment of Chad Basin. *Dutse Journal of Pure and Applied Sciences (DUJOPAS)*, 7, 189-202. doi:<https://dx.doi.org/10.4314/dujopas.v7i4b.20>
- Jamaluddeen, S. S., Aku, M. O., Saleh, M., Bunawa, A. A., & Sharafa, S. B. (2019). A reconnaissance study to delineate the potential mineral zones around the schist belt areas Of Kano State, Nigeria using airborne magnetic data. *Journal of Geology and Mining Research*, 14-21. doi:DOI: 10.5897/JGMR2018.0307
- Lowrie, W. (2007). *Fundamentals of Geophysics*. Cambridge University Press.
- Nazaripour, H., Sedaghat, M., Shafaie, V., & Rad, M. M. (2024). Strategic assessment of groundwater potential zones: a hybrid geospatial approach. *Applied Water Science*. doi:<https://doi.org/10.1007/s13201-024-02243-x>
- Nigerian Geological Survey Agency. (2007). *Survey Specifications*. Abuja: NGSA.
- Ogah, A. J., & Abubakar, F. (2024). Solid mineral potential evaluation using integrated aeromagnetic & aeroradiometric datasets. *Scientific Reports*, 14(1637). doi:<https://doi.org/10.1038/s41598-024-52270-6>
- Rahimi, N., Kargaranbafghi, F., Shahid, M. R., & Afkhami, S. (2024). Using fuzzy Logic Method and Analytic Hierarchy Process to Mineral Potential Mapping in Janja Exploration Area (South of Nehbandan, Iran). *Jordan Journal of Earth and Environmental Sciences*, 15(4), 275-286.
- Taofeeq, O. L. (2021). Integrated aeromagnetic and aeroradiometric data for delineating lithologies, structures, and hydrothermal alteration zones in part of nouthwestern Nigeria. *Asian Journal of Geological Research*, 4(2), 1-16. Retrieved from <http://www.sdiarticle4.com/review-history/67062>
- Telford, W. M., Geldart, L. P., & Sheriff, R. E. (1990). *Applied Geophysics*. Cambridge University Press. Retrieved from <https://dokumen.pub/applied-geophysics-2nbsped-0521339383-978-0521339384.html>